On the analysis of diffuse reflectance measurements to estimate the optical properties of amorphous porous carbons and semiconductor/carbon catalysts

Getaneh Diress Gesesse, Alicia Gomis-Berenguer, Marie-France Barthe, Conchi Maria Concepcion Ovin Ania

Journal of Photochemistry & Photobiology A: Chemistry 398 (2020) 112622

Contents lists available at ScienceDirect

Journal of Photochemistry & Photobiology A: Chemistry

journal homepage: www.elsevier.com/locate/jphotochem

On the analysis of diffuse reflectance measurements to estimate the optical properties of amorphous porous carbons and semiconductor/carbon catalysts

Getaneh Diress Gesesse, Alicia Gomis-Berenguer, Marie-France Barthe, Conchi O. Ania*

CEMHTI, CNRS (UPR 3079), Université d'Orléans, 45071 Orléans, France

ARTICLE INFO

Keywords:
Optical bandgap estimation
Diffuse reflectance
semiconductor/carbon photocatalyst
Amorphous porous carbons

ABSTRACT

This study provides a critical analysis on the use of diffuse reflectance spectroscopy and Tauc equation to estimate the optical energy bandgap of semiconductor/carbon composites and amorphous porous carbons. Determination of the energy gap from diffuse reflectance is strongly dependent on the analyst's experience, due to uncertainties related to establish the adequate range to fit the experimental data to Tauc equation, and to identify the type of electronic transitions. Furthermore, its application to strong light absorbing or multiphase materials with several absorbing components is not straightforward, due to the appearance of various curvatures/linear ranges. For such, reporting the linear fitting range used in the diffuse reflectance spectra is recommended to avoid miscalculation of a gap value. For materials absorbing in the visible range (e.g., displaced onset in Tauc representation), a double-linear fitting must be used in the extrapolation of $[F(R\infty)hv]^{1/n}$ to avoid underestimation of E_g values. For amorphous porous carbons, different optical responses were obtained from the diffuse reflectance spectra recorded upon dilution with a non-absorbing matrix. The application of Tauc equation (indirect transitions) to data rendered bandgap values ranging between 1.5–2.3 eV for fourteen carbons, which are in agreement with those reported for these materials.

1. Introduction

The use of carbon materials in heterogeneous photocatalysis, either in their role of additives in semiconductor/carbon mixtures or as photocatalysts themselves, has become a largely investigated topic over recent decades [1–3]. Motivated by the low efficiency of most semiconductors under solar light (due to low absorption under visible light, high recombination rates, or photocorrosion issues), the incorporation of a variety of carbons as additives to TiO_2 and other semiconductors has appeared as an effective and simple method to enhance the performance of resulting photocatalyst [1,4–6].

The reasons of the successful performance of the semiconductor/carbon have been discussed based on the nature of the carbon additive itself. For instance, it has been reported that the high electron mobility of nanostructured carbons (e.g., graphene and carbon nanotubes) favors the separation of the photogenerated charge carriers upon delocalization in the π electron density of the carbon matrix (acting as sinks of electrons). Carbon materials would also act as effective photosensitizers due to the high density of C=C double bonds [7–9], which with an adequate functionalization would trigger the harvesting of light in the visible range [10–12]. In the case of porous carbon supports, the rate of the photodegradation reaction is accelerated due to the enhanced mass transfer and confinement of the target molecule in the porosity [1,13,14]. Additionally, carbon nanotubes and nanoporous carbons display self-photoactivity, and are capable of generating reactive oxygen species upon illumination in aqueous suspensions [15–17].

In photocatalytic applications, the optical features of the catalyst play a crucial role in its ability to convert light into chemical reactions. The optical response of a given material is usually estimated by the calculation of its energy gap or bandgap, which represents the energy required to move an electron in a bound state in the valence band to the conduction band, generating electrically bounded electron-hole pairs (e.g. excitons). If the energy input provided by the absorption of photons is high enough to split the excitons (electronic bandgap), they become free charge carriers that can trigger a photocatalytic reaction. In most inorganic semiconductors, both bandgaps are similar due to the low binding energy of the electron–hole pairs [18]; in other cases, as for carbon materials and organic semiconductors differences maybe important due to the high binding energies of the exciton [19–21]. Even though the optical bandgap provides information on a catalyst's

* Corresponding author.
E-mail address: conchi.ania@cnrs-orleans.fr (C.O. Ania).

https://doi.org/10.1016/j.jphotochem.2020.112622
Received 3 April 2020; Received in revised form 6 May 2020; Accepted 7 May 2020
Available online 20 May 2020

threshold for photons to be absorbed, and not necessarily on its electronic bandgap (i.e., threshold for separating the excitons), it is used as a reference parameter to compare catalysts.

Various techniques have been applied for the determination of the optical properties of different materials, such as: electron energy loss, scanning tunneling, UV photoelectron, photothermal deflection, or optical transmittance/absorption/reflectance spectroscopies. Among them, diffuse reflectance spectroscopy is perhaps the most widely used one for semiconductors and semiconductor/carbon mixtures [22–24], as the absorption spectrum of a material gives information on its electronic transitions, and is insensitive to temperature and the electric conductivity of the materials. However, there are important discrepancies in the literature about the nature of the electronic transitions occurring in the materials after the absorption of photons (allowed/forbidden, direct and indirect transitions) that complicate the estimation of the energy gap [25–28]. For instance, in the case of novel semiconductor materials, very often the electronic structure (thus the description of the transitions) remains uncertain or with lack of consensus. In many other cases, discrepancies arise from the improper application of the Kubelka–Munk method [29]; this controversy has long been discussed in the literature for semiconductors (including TiO_2 benchmark) [25–28].

The application of diffuse reflectance spectroscopy for the estimation of the bandgap in semiconductor/carbon composites and carbon materials alone is more complex. This is due to the difficulties associated to rationalize the electronic transitions that occur in semiconductor/carbon composites – that are expected to vary upon the interfacial electronic interactions between the carbon and the semiconductor –, and the strong absorbing nature of the carbon matrix.

The objective of this work is to evaluate the adequateness of the UV–vis diffuse reflectance spectroscopy and the application of the Kubelka–Munk theory and Tauc equation for the estimation of the optical bandgap of semiconductor/carbon composites and of carbon materials. Herein we attempt to provide a critical analysis and some guidelines and recommendations for evaluating the optical bandgap of strong light absorbing catalysts prepared from amorphous carbon materials. While the successful performance of these materials in different fields of photocatalysis has triggered the interest on the evaluation of their optical bandap, there is a lack of common knowledge and/or consensus about the experimental procedures for data acquisition and the adequate representation of the Kubelka-Munk theory of these materials. We will focus on the analysis of diffuse reflectance spectra of semiconductor/carbon composites and of carbon materials, to identify the range to be fitted in the Tauc method, thereby minimizing the subjectivity in the determination of the energy gap (strongly dependent on the analysist's experience); understanding the origin of the optical features of different carbons by establishing a correlation with their physicochemical and/or structural properties is out of the scope of this work.

2. Materials and methods

2.1. Materials

Three semiconductors were selected: TiO_2 (P25, Evonik, Germany), ZnO (Sigma-Aldrich) and Bi_2WO_6 (labelled as BWO) nanopowders, synthesized as reported elsewhere [30]. Several carbon materials with different characteristics were selected. All the materials (carbons, semiconductors and their composites) have been widely characterized in previous works (see details in Table 1 and the Supplementary material). Here, we will reintroduce some structural and physicochemical properties for data interpretation. BWO/carbon and TiO_2/carbon composites were prepared by a physical mixture in a mortar of the carbon and semiconductor powders using a 0.5–13 wt% of carbon material. Unless otherwise stated, the composites are prepared with 2 wt% of carbon additive. The composites were labelled as BWO/X or TiO_2/X, where X stands for the acronym of the carbon additive. For BWO, the carbon additive was also added in a one-step approach during the hydrothermal synthesis of the semiconductor. Such composites are denoted by HS (e.g., BWO/CV HS) [30].

Table 1
Selection of materials used in the study, and their corresponding name in the text.

	Remarks
TiO2	Commercial (P25), Degussa, Evonik
BWO	Bi_2WO_6, hydrothermal synthesis at 140 °C [30]
ZnO	Commercial, Sigma Aldrich
LSM	Coal-derived, steam activation
CNT	Multiwalled Carbon Nanotubes, commercial, Nanocyl
CS	Sucrose-derived hydrochar prepared at 180 °C [31]
Q	Coal-derived, steam activation [32,33]
Qox	Carbon Q oxidized in $(NH_4)_2S_2O_8$ (saturated solution)at room temperature [33]
CV	Biomass, H_3PO_4 activation [32]
CVH450	Carbon CV treated at 450 °C under inert atmosphere for 30 min
CVH850	CV treated at 850 °C under inert atmosphere for 30 min
NoC	Biomass, H_3PO_4 activation [34]
NoCH850	NoC treated at 850 °C under inert atmosphere for 30 min [34]
F	Wood-derived, steam activation, commercial (CPG Carbon) [35]
F6	Carbon F overactivated at 850 °C in CO_2 [35]
F6S	Carbon F6 chemically modified to incorporate S-moieties [35]
T90SUC	Sucrose derived carbon using a silica template
PET-char	Polyethylene terephthalate-derived charcoal [36]
PET-47	PET-char activated at 925 °C in CO_2, up to a burn-off of 47% [36]

2.2. UV–vis diffuse reflectance

The optical features of the photocatalysts were determined by UV–vis diffuse reflectance spectroscopy (Shimadzu UV-2700) in a spectrophotometer equipped with an integrating sphere and using $BaSO_4$ as a blank reference. Measurements were recorded between 200 and 850 nm (due to the configuration of the integrating sphere) in the absorption and diffuse reflectance modes and transformed to a magnitude proportional to the extinction coefficient through the Kubelka–Munk function, $F(R\infty)$ for the estimation of the energy bandgap. Spectra were collected at 1 nm intervals with a spectral bandwidth of 2 nm. Before recording the diffuse reflectance spectra, all the samples were ground in a ball mill to reduce the average particle size below ca. 10 µm. Powders of the samples were pressed in holders of ca. 3 cm diameter and 5 mm depth. In some cases, the powders of the materials were mixed with the reflectance reference ($BaSO_4$) in a mortar- at various weight ratios before recording the diffuse reflectance spectra.

3. Results and discussion

3.1. The Kubelka–Munk theory applied to semiconductors

UV–vis diffuse reflectance spectroscopy is one of the most employed methods for the determination of the optical bandgap of materials. In general, the optical excitation of the electrons provokes an increase in absorbance at the wavelengths corresponding to the activation energy of the electrons, which allows determining the position of the absorption edge. To evaluate the optical bandgap from the absorption spectra, the Kubelka–Munk theory is commonly applied [29]. This theory describes the behavior of the light path through a dispersing medium as a function of the scattering (S) and absorption (k) coefficients:

$$F(R\infty) = (1-R\infty)^2/2R\infty = k/S = \alpha$$

where $F(R\infty)$ is the Kubelka–Munk function corresponding to the absorbance, $R\infty$ is the absolute diffuse reflectance at each wavelength of an infinitely thick sample referred to a non-absorbing standard, k is the

absorption coefficient, S is the scattering coefficient, and α is the absorption coefficient of the material.

The validity of the Kubelka–Munk theory relies on the condition of infinitely thick and densely-packed samples, constituted by randomly-shaped particles whose sizes are comparable to (or smaller than) the wavelength of the incoming radiation. The approximation $F(R\infty) \sim \alpha$ is considered accurate enough for evaluating the optical bandgap of semiconductors from the diffuse reflectance spectra [25,27,37].

For amorphous (or non-crystalline) semiconductors with structural electronic disorder, the optical absorption spectra are characterized by the presence of tail states nearby the valence and conduction bands, and the energy bandgap is usually evaluated from the Tauc representation:

$$\alpha\ h\nu = B\ (h\nu - E_g)^n \text{ or } F(R\infty)\ h\nu = B\ (h\nu - E_g)^n$$

where h is Planck's constant ($4.136\ 10^{15}$ eV s^{-1}), B is an energy independent constant, hν is the photon energy (eV), E_g is the optical bandgap energy (eV), and n is a constant that determines the type of optical transition: n = 2 for indirect allowed transition; n = 3 for indirect forbidden transitions; n = ½ for direct allowed transition; and n = $^3/_2$ for direct forbidden transitions [23,38]. The E_g values can be obtained from the extrapolation of the linear least squares fit of $[F(R\infty)\ h\nu]^{1/n}$ to zero, by plotting $[F(R\infty)\ h\nu]^{1/n}$ vs hν.

Thismethod is simple and convenient for the evaluation of the E_g of amorphous, nano-structured, and mixed-phase poly-crystalline materials [23,39–41]. However, its application and validity is quite controversial. First of all, there is not a unanimous consensus regarding the validity of the mathematical approaches used to fit Tauc equation for data interpretation [25–27]. Another controversial issue is the incertitude concerning the value assigned to the *n* exponent in the Tauc equation. The latter becomes particularly a complex situation for semiconductor/carbon composites and for carbon materials as photocatalysts themselves, since the origin and nature of the electronic transitions remain quite uncertain and are expected to depend on the interactions between the individual components of the composites. In addition, this incertitude is sometimes linked to a common error in the application of a linearized form of Tauc equation that involves the reciprocal value of the exponent (i.e., 1/*n*); this causes a confusion between the values of $n = 2$ (indirect allowed transitions) and $n = 1/2$ (direct allowed transitions) and their corresponding reciprocals (1/*n*): 0.5 and 2, respectively.

The following sections summarize a critical analysis on the usefulness of diffuse reflectance spectroscopy and the Kubelka–Munk theory for the estimation of the energy bandgap in both semiconductor/carbon composites and amorphous carbon materials. Discussion will be driven to compare different experimental procedures for data acquisition and various representations of the Kubelka–Munk theory.

3.2. Optical energy bandgap determination in semiconductors

Fig. 1 shows the diffuse reflectance (DR) spectra of powders of the selected semiconductors (e.g., TiO_2, ZnO, Bi_2WO_6) widely used in the literature in photocatalytic applications, along with the Tauc representations. For all three semiconductors, the DR spectra show an abrupt decrease in the reflectance below 400 nm that is associated to the optical absorption edge of the material. The Tauc representations for the semiconductors display the commonly reported linear dependence of the Kubelka–Munk function with hν, with a smooth function with a low curvature below and above the absorption edge. This allows an easy evaluation of the bandgap as the extrapolation of the linear least squares fit of $[F(R\infty)\ h\nu]^{1/n}$ to zero. For materials with a well-defined absorption edge of the material, the analysis by using a double linear fitting range yields similar extrapolation values (Table 2), thus the main difficulty relies in the choice of the electronic transitions, as it defines the value of the n exponent. Indeed, the energy bandgap values are quite sensitive to the selection of the fitting range and the type of electronic transitions. In our calculations, we have considered indirect transitions for TiO_2 and Bi_2WO_6 (ca. $n = 2$) and direct transitions for ZnO ($n = 1/2$); energy bandgap values of 3.1, 2.9 and 3.3 eV, were obtained, respectively; these values are in agreement with most reported ones for these semiconductors [27,40,42].

Table 2 shows that for a given sample and for the same experimental data, the E_g values varied about ± 0.04 eV for different fitting ranges (all of them linear). The analysis using different electronic transitions changed significantly the calculated bandgap of the semiconductors (ca. 3.6, 3.3 and 3.2 eV when considering direct transitions for TiO_2 and Bi_2WO_6 and indirect transitions for ZnO, respectively). Whenever the electronic transitions of the studied material are not well identified, it would be a good practice to avoid the calculation of the energy gap, to report the experimental diffuse reflectance data and to focus the discussion in the absorption edge.

3.3. Optical energy bandgap determination in semiconductor/carbon composites

Evaluating the optical bandgap of semiconductor/carbon composites is a more complex task, as it depends on various factors such as the absorption features of the individual components, and the composition and synthesis method of the composite, among others. In addition, in the absence of strong interfacial interactions between the semiconductor and the carbon additive, it is reasonable to assume that Tauc equation can be applied assuming that the electronic transitions describing the bare semiconductor are dominant. In contrast, when interfacial interactions between both components cannot be ruled out, a mixed mechanism for the associated electronic transitions could be occurring. In such cases, it would be advisable to gather additional information on the nature of the transitions, and to perform the analysis of the diffuse reflectance data and, more precisely, Tauc representation with care. A few examples are discussed in detail below.

Fig. 2 shows the diffuse reflectance spectra of Bi_2WO_6/carbon and TiO_2/carbon composites with 2 wt% of carbon additive, prepared by different procedures. Discussing the effect of the preparation method of semiconductor/carbon catalysts on their absorption features has been reported elsewhere [30,31] and is out of the scope of this work. We herein reintroduce some properties of certain materials for an adequate analysis of diffuse reflectance spectra that allows to minimize the subjectivity in the determination of the energy gap of semiconductor/carbon composites.

Diffuse reflectance spectra of the composites show the characteristic shape of the semiconductor (either BWO or TiO_2) at around 400 nm for all the samples. The effect of the incorporation of the carbon additive is evidenced by the sharp decrease in the reflectance values above 400 nm for the semiconductor/carbon composites. Interestingly, the DR spectra of series BWO/carbon and BWO/carbon HS (similar composition but different method for incorporating the carbon additive) show a slight blueshift in the absorption edge, and a lower reflectance values for BWO/carbon. The absorption shift, although smaller than that reported for chemically doped and metal-ion implanted semiconductors [43], suggests out the presence of specific interactions with the carbon additive. Differences in the color of the composites were also detected, with lighter colors for the HS series (Fig. S1 in the Electronic Supplementary Information, ESI). This behavior was more pronounced for the composites prepared with carbons CS and CV (both characterized by a high surface functionalization); it has been attributed to the surface interactions between the semiconductor and the functional groups of the carbon additive, that are governed by the nature of the carbon material and the method for preparing the composites, as discussed elsewhere [30]. For both composites BWO/CS HS and BWO/CV HS, the diffuse reflectance spectra of the composites feature the absorption edge above ca. 350 nm, and a second curvature in the profile between 430 and 640 nm. This has been attributed to the presence of chromophoric moieties in the carbon (i.e., photo-sensitive functional groups

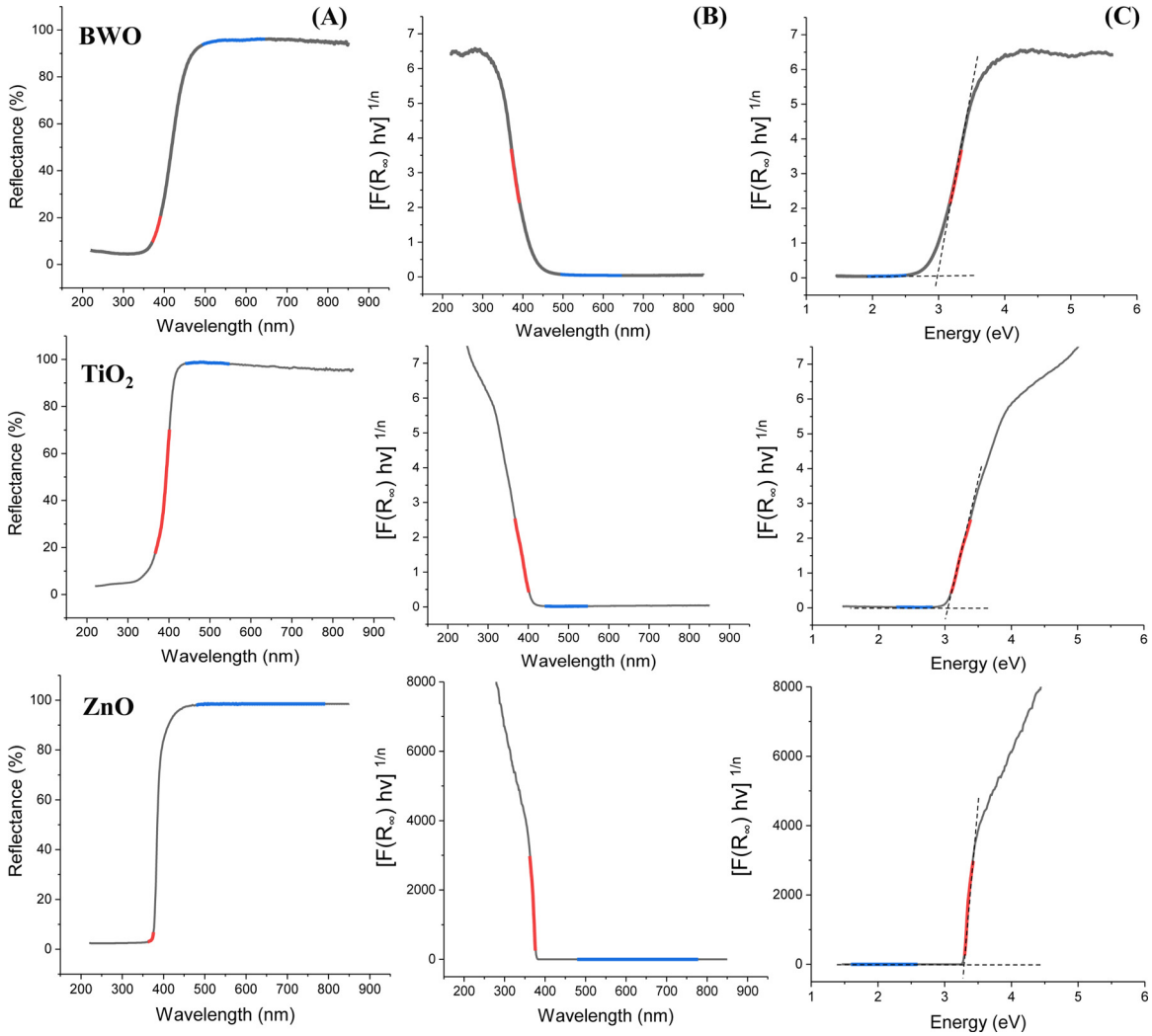

Fig. 1. (A) Diffuse reflectance spectra of BWO, TiO_2 and ZnO semiconductors; (B,C) Optical bandgap calculation from extrapolation of the linear least squares fit of $[F(R\infty)\,hv]^{1/n}$ vs hv using a double fitting approach. $n = 2$ (indirect transitions) was used for BWO, TiO_2; $n = ½$ (direct transitions) was used for ZnO. Experimental data (black line); fitted range (red line); baseline fitting (blue line); dotted lines represent the extrapolation of the double linear fitting ranges (For interpretation of the references to color in this figure citation, the reader is referred to the web version of this article.).

Table 2
Optical bandgap of the three semiconductors, BWO/carbon and TiO_2/carbon composites considering indirect electronic transitions and obtained from upon selection of double linear fitting and zero extrapolation in Tauc representation.

	E_g (eV)[a] Double linear fitting	Fitting range ΔE (meV)	E_g (eV)[a] Zero extrapolation
BWO	2.91 ± 0.03	20	2.93
TiO_2	3.03 ± 0.01	26	3.03
ZnO[b]	3.27 ± 0.01	15	3.27
BWO/CS	3.09 ± 0.04	18	2.78
BWO/Q	3.11 ± 0.03	23	2.82
BWO/CNT	3.12 ± ± 0.02	35	2.19
BWO/CV	3.10 ± 0.02	18	2.55
BWO/Q HS	3.07 ± 0.02	24	2.86
BWO/CS HS[c]	2.90 ± 0.03	20	2.88
BWO/CNT HS	3.11 ± 0.02	25	2.63
BWO/CV HS[c]	3.06 ± 0.04	26	3.05
TiO_2/Q	3.14 ± 0.03	35	3.09
TiO_2/CS	3.12 ± 0.02	30	3.05
TiO_2/CNT	3.25 ± 0.01	34	2.86
TiO_2/CV	3.17 ± 0.02	25	3.09

[a] Correlation coefficients $R^2 > 0.99$ in all cases.
[b] Considering direct transitions.
[c] Evaluated from the first absorption edge above ca. 350 nm (see text).

generally involving O-, N-, S-heteroatoms) that are capable of absorbing light at selected wavelengths in the visible range [10–12,44], and modify the energy levels of the carbon material (compared to the un-functionalized one), facilitating electron transfer reactions [45]. This contribution associated to the transitions in a functionalized carbon matrix is going to be important for the selection of the fitting range in Tauc equation, as it will be discussed below.

Due to the shielding effect of the carbon additive, the diffuse reflectance values of the composites corresponding to the visible range are lower than 100%. As a result, the onset of the Tauc representations is no longer close to zero and appears displaced above the $[F(R\infty)\,hv]^{1/n}$ axis. This is illustrated in Fig. 3 for selected samples; data of all the studied composites are shown in Fig. S2 in the ESI. In these cases, to assure the mathematical consistency of the graphical evaluation of the bandgap, the intersection point to estimate the E_g value can no longer be evaluated by extrapolation of $[F(R\infty)\,hv]^{1/n}$ to zero, and a double-linear fitting must be applied [46]. This practice has also been recommended for samples containing several optical absorbing materials [26].

Even by doing such, the most critical issue in the calculation of the bandgap relies in the selection of the linear range to be fitted. The values calculated for the analyzed semiconductor/carbon composites using various linear fitting ranges are shown in Table 2. As seen, the

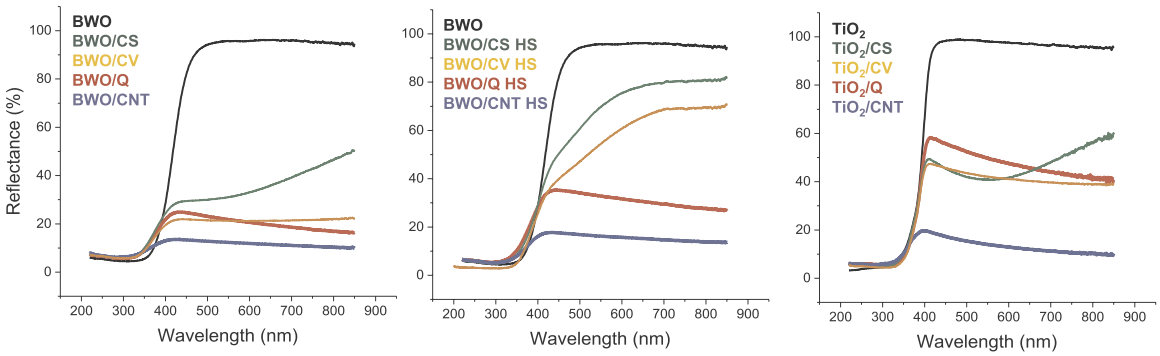

Fig. 2. Diffuse reflectance spectra of the series of semiconductor/carbon composites. Data of the pristine semiconductor is also included as reference.

dispersion of the values for the different fitting ranges accounted for less than 0.05 eV for all the samples. The values of the semiconductor/carbon composites are consistently higher (although differences are subtle) than those of the bare semiconductor for both series. The trend is more pronounced for the carbons of low functionalization (e.g., Q, CNT) and less remarkable for series HS. The higher E_g values for all semiconductor/carbon composites suggests that incorporation of a low amount of carbon (ca. 2 wt%) modifies the optical bandgap of the semiconductor. This is in agreement with the above-mentioned differences in the color of the composites, pointing out to different electron transitions. It also confirms the important role of the synthetic procedure of the catalyst in their absorption features, as different behaviors can be obtained for composites with identical composition prepared by different methods.

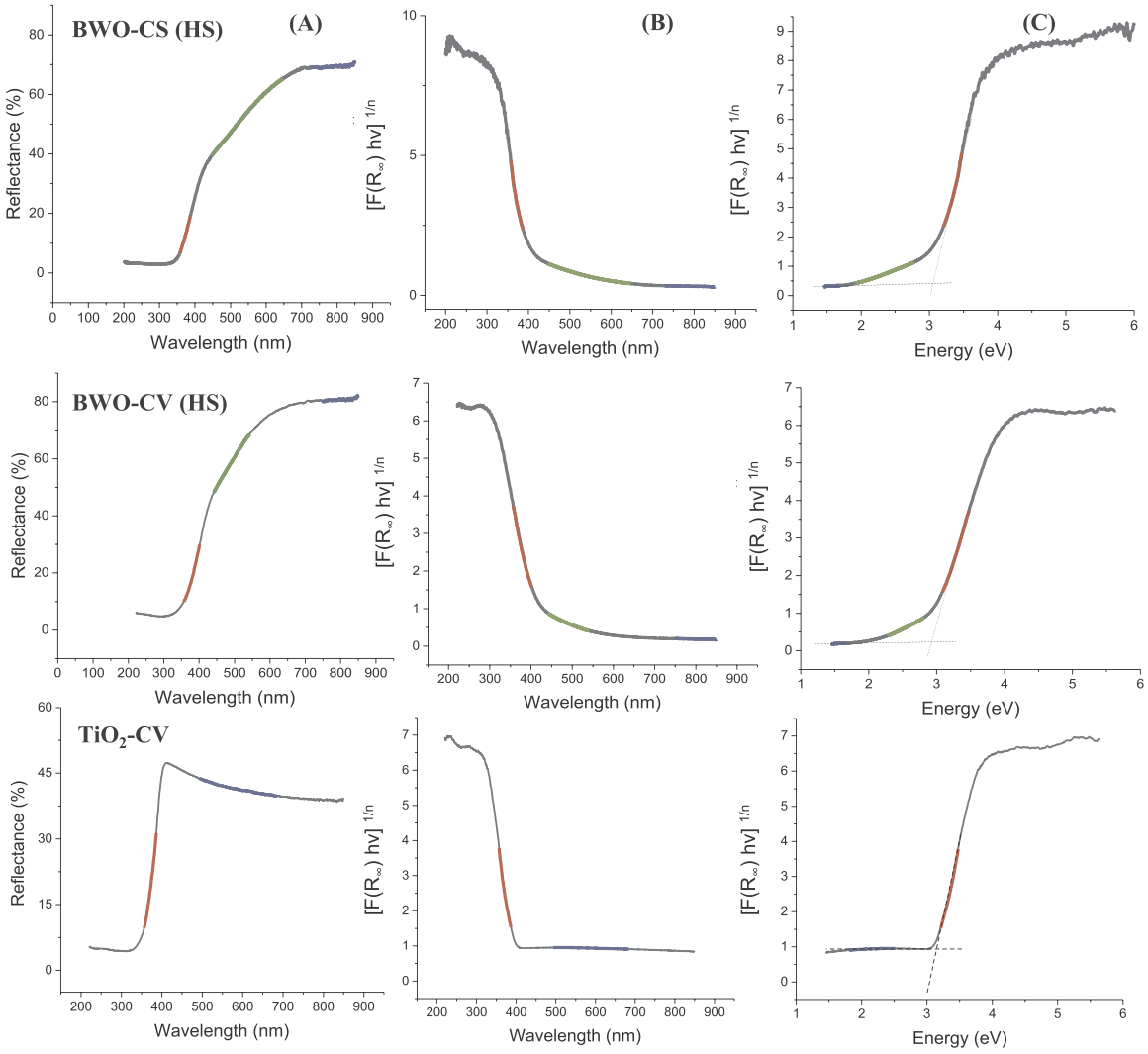

Fig. 3. Diffuse reflectance spectra (A) and (B,C) optical bandgap calculation from extrapolation of the linear least squares fit of $[F(R\infty)\,hv]^{1/n}$ vs hv using double linear fitting in the Tauc representation of selected semiconductor/carbon composites. $n = 2$ (indirect transitions) was used for all the composites. Experimental data (grey line); fitted range (red line); second curvature (light green line); baseline fitting (blue line); dotted lines represent the extrapolation of the double linear fitting ranges (For interpretation of the references to color in this figure citation, the reader is referred to the web version of this article.).

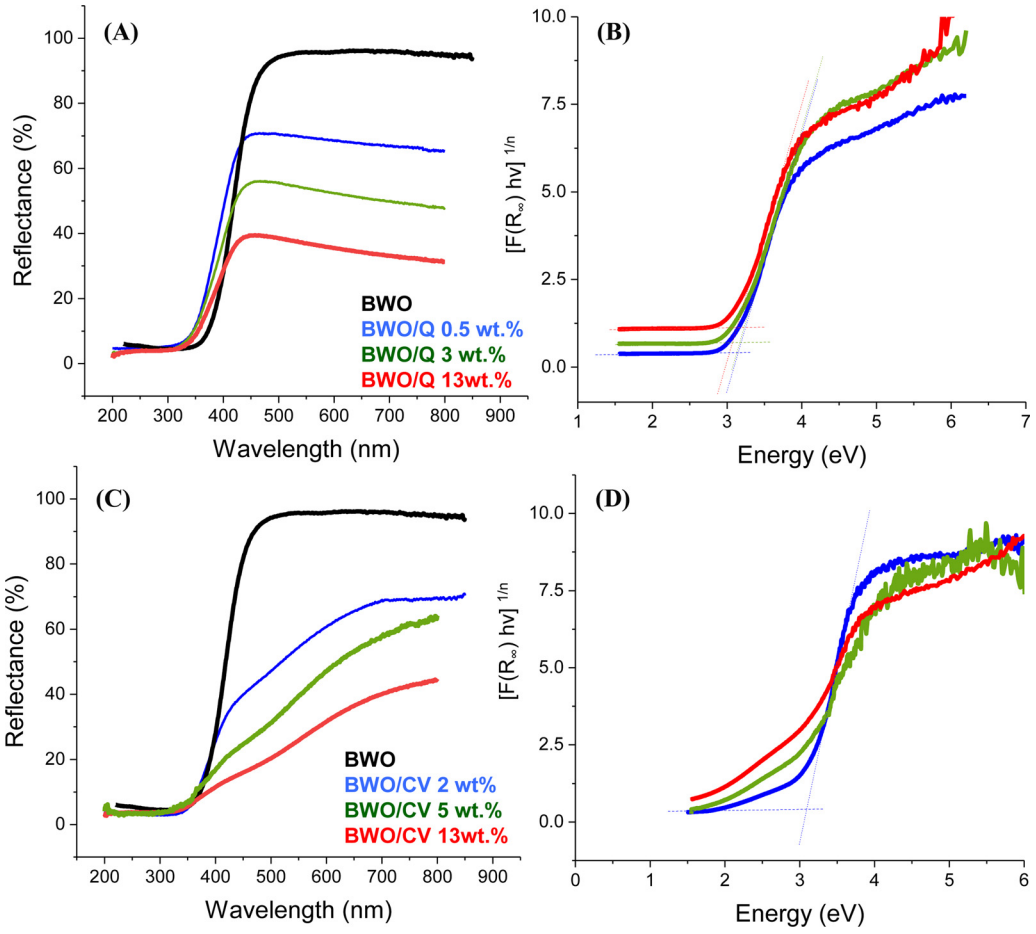

Fig. 4. (A,C) Diffuse reflectance spectra of semiconductor/carbon composites with amount of carbon additive between 0.5 an 13 and 15 wt%; (B,D) Tauc representation and optical bandgap E_g calculation from extrapolation of the linear least squares fit of $[F(R\infty)\ hv]^{1/n}$ vs hv. $n = 2$ (indirect transitions) was used for all the composites; dotted lines represent the extrapolation of the double linear fitting ranges.

Interestingly, Tauc representation of composites BWO/CS HS and BWO/CV HS showed two curvatures that correspond to the well-differentiated zones observed in the diffuse reflectance spectra (Fig. 2). This may suggest that it would be possible to differentiate the contribution of the carbon matrix from that of the semiconductor in the spectra, as it is done for samples containing several optical absorbing materials [26]. Indeed, fitting in the range of 350–400 nm of the first curvature rendered an E_g of 2.90 eV, a value close to that of the pristine semiconductor. On the other hand, fitting between 430 and 700 nm (second curvature assigned to the transitions involving the surface groups of the carbon matrix) yielded an E_g of 2.17 eV. This value is close to the optical bandgaps reported for amorphous carbons (e.g., hydrogenated amorphous carbon films) obtained upon application of the Tauc equation and considering indirect allowed transitions [47,48].

Regarding the amount of carbon in the composites, two different situations are illustrated in Fig. 4. The first one represents the case of a semiconductor/carbon composite prepared with a carbon of low functionalization (e.g. carbon Q) and upon physical mixture of both components – thus, scarce interfacial interactions are expected –. The DR spectra have similar shapes but shifted down to lower reflectance values along the entire spectral range, as a result of the sensitiveness of reflectance to the relative amounts of optical absorbing materials. Despite of this, Tauc representations also show the same shape; accordingly, the estimated energy gap values for the mixtures remained rather constant (ca. 3.1 ± 0.04 eV), with no effect of the amount of carbon (Table S1 in the ESI).

The second example corresponds to a series of composites with increasing amounts of a functionalized carbon additive and prepared via a synthetic method that favors the formation of interfacial interactions between both components (series BWO/CV HS) [30,49]. The DR spectra show that as the amount of carbon increases, the reflectance values decreased, and the second curvature between 430 and 700 nm owing to the absorption of the carbon moieties becomes more pronounced. For the sample with 13 wt% carbon, it becomes less clear to differentiate between the absorption edge of the bare semiconductor – below 430 nm – and the absorption of the carbon groups. Considering the high amount of carbon additive and the synthetic method for the preparation of this composite (i.e., one-pot hydrothermal synthesis of the semiconductor in the presence of a highly functionalized carbon additive), this might be attributed to the occurrence of mixed transitions in the composite. Particularly since the distinctive curvatures in the visible range of the spectra were almost not detected for the same composites prepared upon physical mixture of the individual components. In such cases when it is not possible to accurately isolate the individual contributions of the different phases of a composite, it would be advisable to avoid the estimation of a bandgap. It would be wider to just interpret the optical response of the material upon the description of the experimental DR spectra; and when possible, to provide additional evidence on the nature of the electronic transitions by complementary techniques, rather than calculating E_g values based on uncertain physical phenomena on these materials.

3.4. Optical energy bandgap determination in amorphous carbon materials

While numerous works exist on reporting the optical properties of graphene or carbon nanotubes [50,51], understanding the optical properties of amorphous porous carbon materials is still a challenge, since they often lack of well-defined conduction and valence bands and exhibit a complex structure that differs among carbons (e.g., hybridization state and spatial arrangement of the carbon atoms, surface defects, surface functionalization, porosity). Despite such complexity, recent works reporting the self-photochemical activity of amorphous

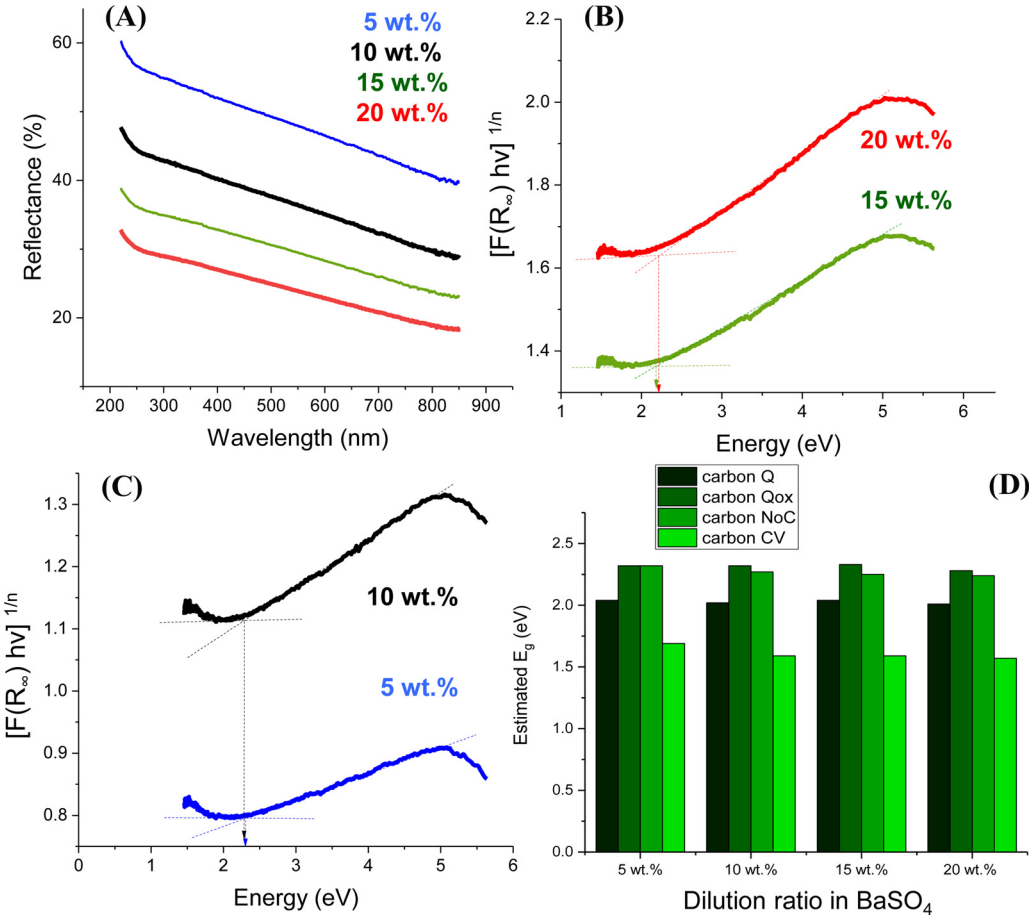

Fig. 5. (A) Diffuse reflectance spectra of various amounts of carbon NoC diluted in $BaSO_4$; (B,C) Example of the optical bandgap calculation from extrapolation of the linear least squares fit of $[F(R\infty)\ hv]^{1/n}$ in the Tauc representation for different dilutions in $BaSO_4$. $n = 2$ (indirect transitions) was used for all the composites; dotted lines represent the extrapolation of the double linear fitting ranges; (D) Variation of the E_g values with the dilution ratio for selected carbons (wt% carbon in $BaSO_4$).

carbons have triggered the research towards exploring and understanding their optical features [52,53]. We herein focus the discussion on the application of diffuse reflectance and Tauc equation to amorphous porous carbons.

Owing to the strong light absorption of carbon materials, the diffuse reflectance spectra of these materials was recorded on the carbons diluted in $BaSO_4$ powders (non-absorbing material used as reflectance standard; 100% reflectance in the full UV–vis range). This is a common practice widely used in the optical characterization of oxides with strong absorption features [24,53,54], based on the fact that reflectance is only sensitive to the relative amount of optical absorbing materials. An example illustrating the validity of this protocol for a semiconductor can be found in Fig. S3 in the ESI. Furthermore, the Kubelka–Munk function is valid for infinitely thick samples that must not transmit any light; this condition is perfectly meet by the carbon/$BaSO_4$ mixtures pressed in millimetric sample holders.

Fig. 5 shows the diffuse reflectance spectra of selected carbons recorded for increasing amounts of carbon diluted in $BaSO_4$, ranging from5 to 20 wt%.

The dilution with barium sulphate does not modify the shape of the spectra, with differences accounting only for the higher reflectance values in the Y-axis as the amount of non-absorbing matrix was raised. The Tauc representations corresponding to the different carbon/$BaSO_4$ mixtures also displayed similar shapes, hence the dilution ratio did not affect the evaluation of the energy gap (Fig. 5), as also reported for other materials [24,54]. Considering this, a dilution of 10 wt% was selected for exploring the absorption features of the selected carbons.

The diffuse reflectance spectra of all the carbons (diluted 10 wt% in $BaSO_4$) are shown in Fig. 6. As seen, all the spectra showed a smooth decrease along the UV–vis range regardless the nature of the carbon, with a steeper decrease in the UV region. These patterns are different from those of inorganic semiconductors such as TiO_2, Bi_2WO_6 or ZnO, for which a sharp reflectance edge (decrease) at wavelengths usually above 400 nm. They indicate that the carbons are capable of absorbing light in the continuum range of wavelength, as opposed to most semiconductors. It should also be noticed that, despite the same dilution was applied to all the samples, the reflectance varied significantly among the studied carbons, ranging from 30 to 70%. This confirms the different ability to absorb light of the studied carbons, which is most likely associated to their physicochemical and structural characteristics. Analyzing the origin of the bandgap in amorphous carbons and its correlation with the properties of these materials remains out of the scope of this study. However, it has been associated to the existence and size of disordered sp^2 domains, the occurrence of σ and π states forming sub-bands, defect tail states introduced upon functionalization, and other structural features (e.g., sp^3 content, dangling bonds) [20,52,55,56].

Regarding the type of electronic transitions, most of the studies report that light absorption processes on amorphous carbons proceed through indirect allowed transitions (thus n = 2) [47,48]. Fewer studies report either direct transitions [53], or the use of exponent 1/n = 0.5 in Tauc representation, without clarifying the type of transitions [21,57–59].

The applicability of Tauc method for the determination of the optical bandgap in carbons has been validated for various types of amorphous carbons [47,48,57,60–64]; most studies agree that Tauc bandgap can be considered a phenomenological parameter to compare. Regardless the type of transition considered, all the curves showed a marked gap, characteristically associated to the optical bandgap. This confirms that the Tauc transformation allows the detection of a bandgap in amorphous carbons.

Considering this, we have fitted the experimental data to Tauc

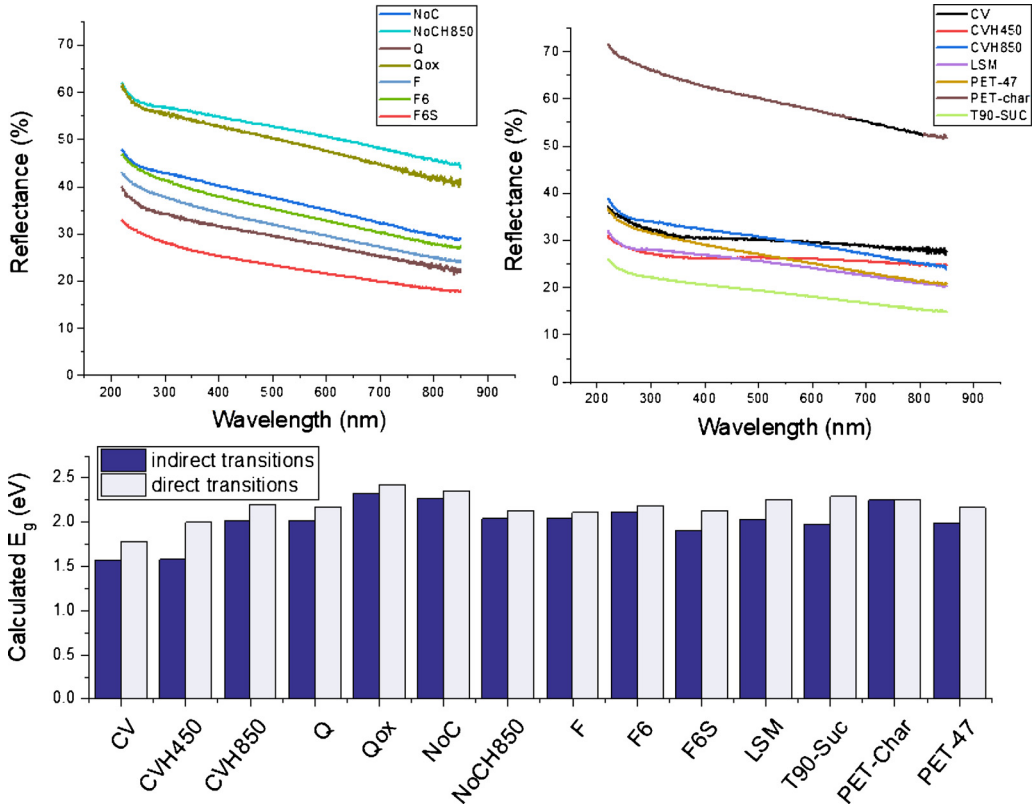

Fig. 6. (top) Diffuse reflectance spectra of the studied carbons diluted with 10 wt% $BaSO_4$; (down) E_g estimated considering both direct and indirect transitions for the selected carbons.

representations using indirect transitions for the carbons (fittings for all the carbons are shown in Fig. S4 in the ESI). Fig. 6 shows the obtained E_g values for the selected carbons; the corresponding Tauc plots and the fitted range for all the analyzed carbons is shown in the ESI. Tauc representations for most of the carbons showed a steep function with a clear linear dependence of $[F(R\infty)\ hv]^{1/n}$ with hv. Only for certain samples (e.g., carbons CV, CVH450, CVH850, FS), the representations displayed a sloping profile characterized by a large absorption tail spanning over a wide range of energies. Although this issue still remains under investigation, it suggests the existence of multi-phonon absorption processes (tail states nearby the valence and conductions bands), as it has been reported for semiconductors with a high structural-electronic disorder [23,25].

The obtained values ranged between 1.5 and 2.2 eV, which are in agreement with those reported for other amorphous carbon with varied functionalization (e.g., 2.2–0.9 eV for hydrogenated amorphous carbon films; 2.4–1.6 eV for N-doped carbon films) [57,61–65] and carbons with varied sp^2/sp^3 ratios (e.g., 4.1 and 1.2 eV for sp^2/sp^3 ratio of 0.16 and 1.63, respectively) [57,66]. They are lower than those reported by Velo-Gala et al. for a series of activated carbons with varied chemical composition (ca. ranging from 3.1 to 3.5 eV) [53], although these authors used direct transitions for data fitting. We have not observed significant variations in the E_g values calculated for indirect and direct transitions (Fig. 6b); despite these similarities, indirect allowed transitions would seem more adequate for describing the electronic transitions involved in amorphous carbons [47,48], based on the number of studies reporting their origin associated to σ and π states [20,52,55,56].

In sum, data should be analyzed with caution to avoid biased calculations of the energy gap in complex materials where the Kubelka–Munk function does not strictly follow a linear dependence with the energy of the photons (sloping functions, multimodal curvatures). In such cases, the graphical validation of the chosen fitting range must be performed not only to assure a consistent mathematical analysis (with high fitting goodness) but that the analysis is carried out in the energy region corresponds to the adequate optical absorption zone of the sample. Whenever this may not be applicable, the calculation of the energy gap should be avoided and the discussion should be centered in the description of the diffuse reflectance spectra and the graphical dependence of the absorption function with hv.

4. Conclusions

Owing to the successful performance of the semiconductor/carbon composites and amorphous porous carbon materials themselves as photocatalysts in various photocatalytic applications, evaluating the optical bandgap of these materials has become a topic of interest in catalysis and materials science, and particularly in the carbon-researching scientific community. While the origin of the optical features of such unconventional semiconductors still remains unclear, researchers have soon adopted the application of diffuse reflectance spectroscopy and Tauc method to calculate energy bandgap values. Even if Tauc bandgap is considered a valid global phenomenological indicator of the potentialities of a material in photocatalytic applications, its calculation is still rather controversial. And its extension to semiconductor/carbon composites and amorphous carbon materials suffers from similar limitations, aggravated by the fact that these materials are strong light absorbing and often multiphase ones. Unambiguity in the description of the optical features of new materials and hybrid composites would be avoided if a cautious analysis of the diffuse reflectance response is carried out. For this, the raw experimental data and the fitting range used for the calculations should be reported, and not just the graphical representation of Tauc equation and the obtained bandgap value as it usually occurs. In the case of materials presenting sloping diffuse reflectance profiles with various curvatures, it is important to assure that the fitting range chosen from the graphical representation of Tauc equation corresponds to the

adequate absorption zone and electronic transitions described. Whenever this may not be applicable, or until a consensus on the type of transitions of carbon-containing catalysts is found an accepted, it would be a good practice to avoid the calculation of the energy gap, or at least to clarify the fitting range used for the calculations in the Tauc representation. For samples with strong absorption features, a mathematically consistent analysis using a double linear fitting should be employed to avoid underestimation of the bandgap values. Measuring the diffuse reflectance spectra of amorphous carbons diluted with a non-absorbing material enables to identify important differences in the optical features of these materials (otherwise unnoticed due to the strong light absorption of the carbon matrix). The analysis of graphical Tauc representation equation in carbons must be done with caution; besides the above-mentioned recommendations, a double linear fitting should be applied for a mathematically consistent analysis avoiding a miscalculation of the bandgap values. Whenever there is uncertainty on the type of transitions (direct or indirect), it would be advisable to clarify the choice made and to support it (if possible) by additional experimental evidences describing the optical response of the material. In our study, bandgap values calculated for a series of twelve carbons with different properties yielded between 1.5 and 2.3 eV, without a significant variation when different types of transitions were applied. However, considering the origin the electronic transitions involved in most amorphous carbons, indirect allowed transitions seem more adequate for these materials.

Authors statement

Getaneh Diress Gesesse: Contributed to data acquisition, analyzed data, contributed to writing the paper.

Alicia Gomis-Berenguer: Contributed to writing the paper.

Marie-France Barthe: Contributed to writing the paper.

Conchi O. Ania: Conceived and designed the manuscript, analyzed and interpreted data, contributed to writing the paper, assembled all the contributions of the authors.

Declaration of Competing Interest

The authors declare no conflict of interest.

Acknowledgements

This work was funded by the European Council Research through a Consolidator Grant (ERC-CoG-648161, PHOROSOL). GDS thanks Region Centre Val de Loire for funding his PhD.

Appendix A. Supplementary data

Supplementary material related to this article can be found, in the online version, at doi:https://doi.org/10.1016/j.jphotochem.2020.112622.

References

[1] R. Leary, A. Westwood, Carbonaceous nanomaterials for the enhancement of TiO2 photocatalysis, Carbon 49 (2011) 741–772.
[2] J.L. Faria, W. Wang, Carbon Materials for Catalysis, Chapter 13, John Wiley & Sons, New York, 2009.
[3] A. Gomis-Berenguer, C.O. Ania, dai, edt., "Metal-Free Nanoporous Carbons in Photocatalysis", Ch. 6, in Carbon-Based Metal-Free Catalysts. Design and Applications vol.2, Wiley-VHC, 2018, p. 760 pp Sept., Print ISBN: 9783527343416; Online ISBN: 9783527811458.
[4] Y. Zhang, Z.R. Tang, X. Fu, Y.J. Xu, TiO_2 – graphene nanocomposites for gas-phase photocatalytic degradation of volatile aromatic pollutant: is TiO_2-graphene truly different from other TiO_2-carbon composite materials? ACS Nano 4 (2010) 7303–7314, https://doi.org/10.1021/nn1024219.
[5] S. Sharma, V. Dutta, P. Singh, P. Raizada, A. Rahmani-Snai, A. Hosseine-Banderghareai, V. Kumar Thakur, Carbon quantum dot supported semiconductor photocatalysts for efficient degradation of organic pollutants in water: a review, J. Clean. Prod. 228 (2019) 755–759, https://doi.org/10.1016/j.jclepro.2019.04.292.
[6] A.S. Mestre, A.P. Carvalho, Photocatalytic degradation of pharmaceuticals carbamazepine, diclofenac, and sulfamethoxazole by semiconductor and carbon materials: a review, Molecules 24 (2019) 3702, https://doi.org/10.3390/molecules24203702.
[7] H.T. Yu, X. Quan, S. Chen, H. Zhao, TiO_2-multiwalled carbon nanotube heterojunction arrays and their charge separation capability, J Phys Chem C 111 (35) (2007) 12987–12991, https://doi.org/10.1021/jp0728454.
[8] G. Williams, B. Seger, P.V. Kamat, TiO2-Graphene Nanocomposites. UV-Assisted Photocatalytic Reduction of Graphene Oxide, ACS Nano 2 (2008) 1487–1491, https://doi.org/10.1021/nn800251f.
[9] W. Wang, P. Serp, P. Kalck, J.L. Faria, Visible light photodegradation of phenol on MWNT-TiO2 composite catalysts prepared by a modified sol-gel method, J. Mol. Catal. A Chem. 235 (2005) 194–199, https://doi.org/10.1016/j.molcata.2005.02.027.
[10] T.J. Bandosz, J. Matos, M. Seredych, M.S.Z. Islam, R. Alfano, Photoactivity of S-doped nanoporous activated carbons: a new perspective for harvesting solar energy on carbon-based semiconductors, Appl. Catal. A Gen. 445-446 (2012) 159–165, https://doi.org/10.1016/j.apcata.2012.08.020.
[11] J. Matos, A. Garcia, M.M. Titirici, Solvothermal carbon-doped TiO_2 photocatalyst for the enhanced methylene blue degradation under visible light, Appl. Catal. A-Gen. 390 (2010) 175–182, https://doi.org/10.1016/j.apcata.2010.10.009.
[12] A. GomisBerenguer, M. Seredych, J.C. Lima, J. Iniesta, T.J. Bandosz, C.O. Ania, Sulfur-mediated photochemical energy harvesting in nanoporous carbons, Carbon 104 (2016) 253–259, https://doi.org/10.1016/j.carbon.2016.02.058.
[13] J. Matos, J. Laine, J.M. Herrmann, Synergy effect in the photocatalytic degradation of phenol on a suspended mixture of titania and activated carbon, Appl. Catal. B-Environ. 18 (1998) 281–291.
[14] N.G. Asenjo, R. Santamaría, C. Blanco, M. Granda, P. Álvarez, R. Menéndez, Correct use of the Langmuir–Hinshelwood equation for proving the absence of a synergy effect in the photocatalytic degradation of phenol on a suspended mixture of titania and activated carbon, Carbon 22 (2013) 62–69, https://doi.org/10.1016/j.carbon.2012.12.010.
[15] Y. Luo, Y. Heng, X. Dai, W. Chen, J. Li, Preparation and photocatalytic ability of highly defective carbon nanotubes, J. Solid State Chem. 182 (2009) 2521–2525, https://doi.org/10.1016/j.jssc.2009.07.010.
[16] L.F. Velasco, E. Maurino, E. Laurenti, I.M. Fonseca, J.C. Lima, C.O. Ania, Photoinduced reactions occurring on activated carbons. A combined photooxidation and ESR study, Appl. Catal. A-Gen. 452 (2013) 1–8, https://doi.org/10.1016/j.apcata.2012.11.033.
[17] I. Velo-Gala, J. López-Penalver, M. Sánchez-Polo, J. Rivera-Utrilla, Role of activated carbon surface chemistry in its photocatalytic activity and the generation of oxidant radicals under UV or solar radiation, Appl. Catal. B: Environ. 207 (2017) 412, https://doi.org/10.1016/j.apcatb.2017.02.028.
[18] H. Bassler, Excitonic model versus band gap model in organic materials: theory, Encycl. Mater. Sci. Technol. (Second Ed.) (2001) 2825–2829, https://doi.org/10.1016/B0-08-043152-6/00504-0.
[19] M. Knupfer, Exciton binding energies in organic semiconductors, Appl. Phys. A 77 (2003) 623–626, https://doi.org/10.1007/s00339-003-2182-9.
[20] J. Robertson, E.P. O'Reilly, Electronic and atomic structure of amorphous carbon, Phys. Rev. B 35 (1987) 2946, https://doi.org/10.1103/PhysRevB.35.2946.
[21] D. Dasgupta, F. Demichelis, C.F. Pirri, A. Tagliaferro, Pi bands and gap states from optical absorption and electronspin resonance studies on amorphous carbon and amorphous hydrogenated carbon films, Phys. Rev. B Condens. Matter 43 (3) (1991) 2131–2135, https://doi.org/10.1103/physrevb.43.2131 15.
[22] P.D. Fochs, The measurement of the energy gap of semiconductors from their diffuse reflection spectra, Proc. Phys. Soc. (Sec. B) 69 (1) (1956) 70–75.
[23] A.R. Zanatta, I. Chambouleyron, Absorption edge, band tails, and disorder of amorphous semiconductors, Phys. Rev. B 53 (1996) 3833–3836, https://doi.org/10.1103/PhysRevB.53.3833.
[24] R.W. Frei, Diffuse Reflectance Spectroscopy Environmental Problem Solving, CRC Press, London, 2018.
[25] A.R. Zanatta, Revisiting the optical bandgap of semiconductors and the proposal of a unified methodology to its determination, Sci. Rep. 9 (2019) 78, https://doi.org/10.1038/s41598-019-47670-y.
[26] A. Escobedo-Morales, I.I. Ruiz-Lopez, Mde L. Ruiz-Peralta, L. Tepech-Carrillo, M. Sanchez-Cantu, J.E. Moreno-Orea, Automated method for the determination of the band gap energy of pure and mixed powder samples using diffuse reflectance spectroscopy, Heliyon 5 (2019) e01505 e01505 https://10.1016/j.heliyon.2019.
[27] R. López, R. Gómez, Band-gap energy estimation from diffuse reflectance measurements on sol-gel a comparative study, J. Sol-Gel Sci. Technol. 61 (1) (2012) 1–7, https://doi.org/10.1007/s10971-011-2582-9.
[28] S. Bock, C. Kijatkin, D. Berben, M. Imlau, Absorption and remission characterization of pure, dielectric (nano-)powders using diffuse reflectance spectroscopy: an end-to-end instruction, Appl. Sci. 9 (22) (2019) 4933, https://doi.org/10.3390/app9224933.
[29] P. Kubelka, F. Munk, Ein beitrag zur optik der farbanstriche, Z. Techn. Physik 12 (1931) 593–601.
[30] R.J. Carmona, L.F. Velasco, M.C. Hidalgo, J.A. Navio, C.O. Ania, Boosting the visible-light photoactivity of Bi_2WO_6 using acidic carbon additives, Appl. Catal. A Gen. 505 (2015) 467–477, https://doi.org/10.1016/j.apcata.2015.05.011.
[31] L.F. Velasco, M. Haro, J. Parmentier, R. Gadiou, C. Vix-Guterl, C.O. Ania, Tuning the phtocatalytic activity and optical properties of mesoporous TiO_2 spheres by carbon scaffold, J. Catal. 178512 (2013), https://doi.org/10.1155/2013/178512.
[32] L.F. Velasco, I.M. Fonseca, J.B. Parra, J.C. Lima, C.O. Ania, Photochemical behaviour of activated carbons under UV irradiation, Carbon 50 (2012) 249–258,

https://doi.org/10.1016/j.carbon.2011.08.042.
[33] L.F. Velasco, C.O. Ania, Understanding phenol adsorption mechanisms on activated carbons, Adsorption 17 (2011) 247–254, https://doi.org/10.1007/s10450-011-9322-x.
[34] C.O. Ania, B. Cabal, C. Pevida, A. Arenillas, J.B. Parra, F. Rubiera, J.J. Pis, Effects of activated carbon properties on the adsorption of naphthalene from aqueous solutions, Appl. Surf. Sci. 253 (2007) 5741–5746, https://doi.org/10.1016/j.apsusc.2006.12.036.
[35] A. Gomis-Berenguer, J. Iniesta, V. Maurino, J.C. Lima, C.O. Ania, Nanoconfinement and wavelength dependence of the photochemistry of nanoporous carbons, Carbon 96 (2016) 98–104, https://doi.org/10.1016/j.carbon.2015.09.047.
[36] J.B. Parra, C.O. Ania, A. Arenillas, F. Rubiera, J.J. Pis, J.M. Palacios, Characterization of activated carbons obtained by pyrolysis and CO_2 activation of polyethyleneterephthalate wastes, Adsorpt. Sci. Technol. 24 (7) (2007) 439–450, https://doi.org/10.1016/S0167-2991(02)80178-1.
[37] A.B. Murphy, Bandgap determination from diffuse reflectance measurements of semiconductor films, and application to photoelectrochemical water-splitting, Sol. Energy Mater. Sol. Cells 91 (14) (2007) 1326–1337, https://doi.org/10.1016/j.solmat.2007.05.005.
[38] J. Tauc, R. Grigorovici, A. Vancu, Optical properties and electronic structure of amorphous germanium, Phys Status Solidi 15 (2) (1966) 627–637, https://doi.org/10.1002/pssb.19660150224.
[39] A. Dolgonos, T.O. Mason, K.R. Poeppelmeier, Direct optical band gap measurement in polycrystalline semiconductors: a critical look at the Tauc method, J. Solid State Chem. 240 (2016) 43–48, https://doi.org/10.1016/j.jssc.2016.05.010.
[40] N. Satoh, T. Nakashima, K. Kamikura, K. Yamamoto, Quantum size effect in TiO_2 nanoparticles prepared by finely controlled metal assembly on dendrimer templates, Nat. Nanotecnol. 3 (2008) 106–111, https://doi.org/10.1038/nnano.2008.2.
[41] E.M. Vinod, K. Ramesh, K.S. Sangunni, Structural transition and enhanced phase transition properties of Se doped $Ge_2Sb_2Te_5$ alloys, Sci. Rep. 5 (2015) 8050, https://doi.org/10.1038/srep08050.
[42] K.M. Reddy, S.V. Manoramaa, A.R. Reddy, Bandgap studies on anatase titanium dioxide nanoparticles, Mater. Chem. Phys. 78 (1, 3) (2003) 239–245, https://doi.org/10.1016/S0254-0584(02)00343-7.
[43] M. Anpo, M. Takeuchi, The design and development of highly reactive titanium oxide photocatalysts operating under visible light irradiation, J. Catal. 216 (2003) 505–516, https://doi.org/10.1016/S0021-9517(02)00104-5.
[44] R. Ocampo-Pérez, M. Sánchez-Polo, J. Rivera-Utrilla, R. Leyva-Ramos, Enhancement of the catalytic activity of TiO2 by using activated carbon in the photocatalytic degradation of cytarabine, Appl. Catal. B Environ. 104 (2011) 177–184, https://doi.org/10.1016/j.apcatb.2011.02.015.
[45] V.V. Strelko, V.S. Kuts, P.A. Thrower, On the mechanism of possible influence of heteroatoms of nitrogen, boron and phosphorous in a carbon matrix on the catalytic activity of carbons in electron transfer reactions, Carbon 38 (2000) 1499–1524, https://doi.org/10.1016/S0008-6223(00)00121-4.
[46] G.H. Chan, B. Deng, M. Bertoni, J.R. Ireland, M.C. Hersam, T.O. Mason, R.P. Van Duyne, J.A. Iberse, Syntheses, structures, physical properties, and theoretical studies of CeMxOS (M = Cu, Ag; x ≈ 0.8) and CeAgOS, Inorg. Chem. 45 (2006) 8264–8272, https://doi.org/10.1021/ic061041k.
[47] J.F. Yu, T.S. Chen, H.C. Lin, S.T. Shiue, The effect of rapid thermal annealing on characteristics of carbon coatings on optical fibers, Phys. Status Solidi A 207 (2010) 379, https://doi.org/10.1002/pssa.200925345.
[48] A. Foulain, Annealing effects on optical and photoluminescence properties of a-C : H films, J. Phys. D Appl. Phys. 36 (2003) 394, https://doi.org/10.1088/0022-3727/36/4/311.
[49] A. Gomis-Berenguer, I. Eliani, V.F. Lourenço, R.J. Carmona, L.F. Velasco, C.O. Ania, Insights on the use of carbon additives as promoters of the visible-light photocatalytic activity of Bi2WO6, Mol. Mater. 12 (2019) 385–399, https://doi.org/10.3390/ma12030385.
[50] M.A. Rashid Yusoff, Graphene Optoelectronics: Synthesis, Characterization, Properties, and Applications, Wiley-VCH, Baden-Württemberg,2014.
[51] A. Jorio, G. Dresselhaus, Carbon Nanotubes: Advanced Topics in the Synthesis, Structure, Properties and Applications (Topics in Applied Physics), Book 111, Springer, New York 2008.
[52] T.J. Bandosz, C.O. Ania, Origin and perspectives of the photochemical activity of nanoporous carbons, Adv. Sci. 5 (2018) 1800293–1800315, https://doi.org/10.1002/advs.201800293.
[53] I. Velo-Gala, J. López-Penalver, M. Sánchez-Polo, J. Rivera-Utrilla, Surface modifications of activated carbon by gamma irradiation, Carbon 67 (2014) 236–249, https://doi.org/10.1016/j.carbon.2013.09.087.
[54] B. Karvaly, I. Hevesi, Investigations on diffuse reflectance spectra of V2O5 powder, Z. Naturforschung A 26 (2) (1970) 394, https://doi.org/10.1515/zna-1971-0211.
[55] J. Robertson, Mechanical properties and coordinations of amorphous carbons, J. Phys. Rev. Lett. 68 (1992) 220, https://doi.org/10.1103/PhysRevLett.68.220.
[56] A.D. Modestov, J. Gun, O. Lev, Graphite photoelectrochemistry study of glassy carbon, carbon-fiber and carbon-black electrodes in aqueous electrolytes by photocurrent response, Surf. Sci. 417 (1998) 311–322, https://doi.org/10.1016/S0039-6028(98)00681-5.
[57] S. Adhikari, H.R. Aryal, D.C. Ghimire, G. Kalita, M. Umeno, Optical band gap of nitrogenated amorphous carbon thin films synthesized by microwave surface wave plasma CVD, Diamond Relat. Mater. 17 (2008) 1666–1668, https://doi.org/10.1016/j.diamond.2008.03.027.
[58] N. Ahmad, N.A. Tahir, M. Rusop, Amorphous carbon thin films deposited by Thermal CVD using camphoric carbon as precursor, Adv. Mater. Res. 403-408 (2012) 646–650, https://doi.org/10.4028/www.scientific.net/AMR.403-408.646.
[59] G. Fanchini, S.C. Ray, A. Tagliaferro, Optical properties of disordered carbon-based materials, Surf. Coat. Technol. 151–152 (2002) 233–241.
[60] M.-L. Theye, V. Paret, Spatial organization of the sp^2-hybridized carbon atoms and electronic density of states of hydrogenated amorphous carbon films, Carbon 40 (2002) 1153, https://doi.org/10.1016/S0008-6223(01)00291-3.
[61] D.A. Anderson, The electrical and optical properties of amorphous carbon prepared by the glow discharge technique, Philos. Mag. 35 (1977) 17–26, https://doi.org/10.1080/14786437708235968.
[62] B. Dischler, A. Bubenzer, P. Koidl, Hard carbon coatings with low optical absorption, Appl. Phys. Lett. 42 (1983) 636, https://doi.org/10.1063/1.94056.
[63] J. Fink, T. Mdller-Heznzerling, J. Pflfiger, A. Bubenzer, P. Koidl, G. Crecelius, Structure and bonding of hydrocarbon plasma generated carbon films: an electron energy loss study, Solid State Commun. 47 (1983) 687, https://doi.org/10.1016/0038-1098(83)90635-X.
[64] B. Meyerson, F.W. Smith, Electrical and optical properties of hydrogenated amorphous carbon films, J. Non-Cryst. Solids 35-36 (1980) 435–440, https://doi.org/10.1016/0022-3093(80)90633-X.
[65] Y. Miyajima, Y. Tison, C.E. Giusca, V. Stolojan, H. Watanabe, H. Habuchi, S.J. Henley, J.M. Shannon, S.R.P. Silva, Probing the band structure of hydrogen-free amorphous carbon and the effect of nitrogen incorporation, Carbon 49 (2011) 5229–5238.
[66] S. Kaplan, F. Jansen, M. Machonkin, Characterization of amorphous carbon-hydrogen films by solid-state nuclear magnetic resonance, Appl. Phys. Lett. 47 (1985) 750, https://doi.org/10.1063/1.96027.